

Dark matter, neutrino mass and baryogenesis in the radiative seesaw model

Pritam Das,^{1,*} Mrinal Kumar Das,^{1,†} and Najimuddin Khan^{2,‡}

¹*Department of Physics, Tezpur University, Assam-784028, India*

²*School of Physical Sciences, Indian Association for the Cultivation of Science 2A & 2B, Raja S.C. Mullick Road, Kolkata 700032, India*

We study the simplest viable dark matter model with an additional neutral real singlet scalar, including a vectorlike singlet and doublet fermions. We find a considerable enhancement in the allowed region of the scalar dark matter parameter spaces in the presence of these fermions. The decay of the lightest component of the fermion doublet enhances the lepton number violating process, which produces sufficient lepton number asymmetry in the strong wash-out regime. It helps to explain baryogenesis via the mechanism of thermal leptogenesis. This model could also accommodate tiny neutrino masses and mixing at one loop-level through the radiative seesaw mechanism. Dilepton+ \cancel{E}_T signature arising from the new fermionic sector can observe at Large Hadron Collider (LHC), satisfying relic density, including other theoretical and experimental bounds. We perform such analysis for a benchmark point in the context of 14 TeV LHC experiments with a future integrated luminosity of 3000 fb^{-1} .

I. INTRODUCTION

Pieces of evidence from various astrophysical observations like gravitational lensing effects in Bullet cluster, anomalies in the galactic rotation curves, etc., have confirmed the existence of dark matter (DM) in the Universe. Since no particle within the SM has adequate properties to play the role of DM, we must go beyond the SM in the search of new physics. The recent LHC Higgs signal strength data [1, 2] also suggests that one can have rooms for the new physics beyond the SM. To address DM within BSM, various possibilities have been proposed in Refs. [3] and references therein. However, adding a few numbers of fields to the SM, among which the lightest is neutral and stable due to the imposed discrete Z_n and/or Z_n -type ($n \geq 2$, integer) symmetry is the popular one. Heavy scalars or neutrinos, which can behave as weakly interacting massive particles (WIMPs) are the most auspicious candidate as their cross-section results match to be produced as a thermal relic with the observed density. Rich literature on minimal models of DM considering scalar and fermion multiplets are available today [4–8]. In particular, the addition of scalar singlet and fermion singlet, as well as doublet in a minimal model, have rich demand in DM study. As, the mixing of fermion doublet and singlets reduces the coupling to weak gauge bosons and can transform DM from a Dirac into a Majorana particle, yielding the correct relic density with allowed direct detection cross-section [9].

To date, we still can not see any sign of the dark

matter from various direct detection experiments. Recent Xenon-1T experiment [10] puts stringent bounds on the dark matter portal interaction strength(s). DM detection experiments indicate that either dark matter may interact with the nucleus very feebly (detection cross-section could reach beyond the line of neutrino floor [11, 12]) or the interaction is completely zero. The dark matter annihilation into the SM particles via s -channels may absent. On the other hand, if nature has only one-component dark matter then the H - and Z -bosons portal dark matter models may not be the right one to give the exact relic density. It is already known from the literature [13–16] that in the presence of another particles one can get the exact relic density via the co-annihilation channels. One may have the interaction terms in such a way that the dark matter can annihilate into the SM particles via the t - or u -channels, which help to modify the effective annihilation cross-section to give the exact relic density. These types of scenarios can be achieved in the proposed minimal model which gives the correct dark matter density satisfying all the other theoretical and experimental constraints.

At the current Universe, there is an asymmetry in baryon number is observed. Meanwhile, various established suggestions regarding the evolution of our Universe confirm that at the very beginning, there were equal numbers of matter and corresponding anti-matter. This scenario can be explained by the process which is popularly known as baryogenesis. Numerical definition for baryon asymmetry at current date reads as [17], $Y_{\Delta B} (\equiv \frac{n_B - n_{\bar{B}}}{s} \Big|_0) = (8.75 \pm 0.23) \times 10^{-11}$, where n_B , $n_{\bar{B}}$ and s are the number densities of, respectively, baryons, antibaryons and entropy, a subscript *zero* implies ‘at present time’. The numerical value is from the combined microwave background and large scale

* Email Address:prtmDas9@gmail.com

† Email Address:mkdDas@tezu.ernet.in

‡ Email Address:khanphysics.123@gmail.com

structure data [18]. The SM does not have enough ingredient (three Sakharov conditions [19]) to explain this asymmetry, hence BSM frameworks become ideal for accommodating baryogenesis. An attractive way to explain baryogenesis is via the mechanism of thermal leptogenesis [17, 20]. Thermal Leptogenesis is close to type-I seesaw, and together they possess rich literature [17, 19, 21–25]. In the process of thermal leptogenesis, the out-of-equilibrium decay of the lightest right-handed neutrino (RHN) produces sufficient lepton asymmetry that converted into baryon asymmetry via the spharelon process [26]. A vital limitation in this process is that it demands a very high scale of RHN mass (above 10^8 GeV) to make the process work [25, 27]. The large RHN mass scale in standard thermal leptogenesis is because of the CP asymmetry in RHN decays is proportional to the product of active and RHN masses [28]. However, these large RHN masses are not welcome due to several reasons. First of all, these many mass scales are unable to probe at on-going collider experiments [29] and low-scale leptogenesis might rule out lepton numbers at high scale [30, 31]. Second, for higher RHN mass, the naturalness problem arises due to the fine-tuning of the SM Higgs mass parameter [32]. Thus it would be more alluring to construct such a model where low-scale leptogenesis might be feasible. Various studies for low-scale leptogenesis has been carried out along with the scotogenic model [31, 33, 34]. Most of the studies were focused on the decay of right-handed Majorana neutrino that produces sufficient lepton asymmetry whereas we have considered the decay of a vectorlike fermion (VLF). The decay of the VLF into a lepton and scalar violates the lepton number by two units hence lepton asymmetry is generated.

In the model-building prospect, models that can address many SM shortfalls are more appealing and well-motivated also. A dark matter model is said to be completed only when it can simultaneously explain light neutrino observable. It would be more attractive if one can establish a relation between dark matter and light neutrino parameters. In this current work, we have not only introduced a viable dark matter candidate but also tried to address the tininess of neutrino mass generation and baryogenesis in a single framework. The framework that is popular in accommodating both dark matter and neutrino mass is known as the *scotogenic* model, first proposed by Ma [8], where the dimension-5 operator is realized in one-loop level. The notable feature of this framework is the way it connects neutrino and DM. Due to the additional Z_2 discrete symmetry, new fields that contribute to the loop to produce sizable neutrino mass, acquire opposite parity to the SM fields, hence become stable and can be addressed as a viable dark matter candidate. Due to its convincing features in address-

ing neutrino and dark matter, the scotogenic model has gained popularity over time [34–38].

Keeping these in view, we consider a minimal model of DM comprise of a vectorlike singlet and doublet fermion along with a singlet scalar. Apart from the SM $SU(2)$ and $U(1)$, an additional Z_2 symmetry is introduced. All new fields are assigned odd under Z_2 -symmetry such that an odd number of BSM particles do not couple with the SM particles. The scalar singlet in this model is behaving as dark matter on the other hand the charged component of the fermion doublet is taking part in lepton number violation processes. The charged VLFs mixes via a mixing angle β . This mixing angle, couplings, masses, etc. play a significant role in dark matter, neutrino, leptogenesis phenomenology and in collider searches. Moreover, the interaction of vectorlike fermions with SM fields makes them more comfortable to probe in collider searches. We look for collider signature for the lightest charged fermion in the context of 14 TeV LHC experiments with a future luminosity of 3000fb^{-1} for $pp \rightarrow E_1^\pm E_1^\pm$ event processes which yield dilepton plus large transverse missing energy \cancel{E}_T (arising from the dark matter) in the final state. To the best of our knowledge, the detailed analysis of this model has not yet been done in the literature which motivates us to do the analysis.

The rest of the work is organized as follows. We have given the complete model description in section II. Constraints from various sources on this model are discussed in section III. Numerical analysis from dark matter, baryogenesis and collider searches are discussed under section IV and finally we have concluded our work in section V.

II. MODEL FRAMEWORK

The model addressed here, contains (i) a real scalar singlet (S), (ii) a vectorlike charged fermion singlet E_S^- and (ii) a vectorlike fermion (VF) doublet, $F_D = (X_1^0 \ E_D^-)^T$. The charge content of the fields are given in the table I. It is to be noted that these additional

Symmetries	S	F_D	E_S
$SU(2)$	1	2	1
$U(1)_Y$	0	-1	-2
Z_2	-1	-1	-1

TABLE I: Field content and their charges under three different symmetries. S represents the scalar singlet while F_D and E_S are fermion doublet and singlet respectively.

fermions are vectorlike and hence, they do not introduce any extra anomalies in the theory [39, 40]. The SM satisfies the anomaly free condition because of the presence of a quark family to each lepton family. The additional vector-like fermions used here, have the right chiral components transforming similarly to the left chiral ones under the SM gauge symmetry. Therefore, the model is anomaly free. All the BSM particles are considered odd under the discrete Z_2 symmetry, such that, this BSM field does not mix with the SM fields. As a result, the lightest and neutral particle is stable and considered to be a viable dark matter candidate. Let us now elaborate on the model part in detail. The Lagrangian of the model read as,

$$\mathcal{L} = \mathcal{L}_{\text{SM}} + \mathcal{L}_S + \mathcal{L}_{\mathcal{F}} + \mathcal{L}_{\text{int}}. \quad (1)$$

where,

$$\mathcal{L}_S = \frac{1}{2}|\partial_\mu S|^2 - \frac{1}{2}kS^2\phi^2 - \frac{1}{4}m_S^2S^2 - \frac{\lambda_S}{4!}S^4 \quad (2)$$

$$\mathcal{L}_{\mathcal{F}} = \overline{F}_D\gamma^\mu D_\mu F_D + \overline{E}_S\gamma^\mu D_\mu E_S - M_{ND}\overline{F}_D.F_D - M_{NS}\overline{E}_S.E_S. \quad (3)$$

$$\mathcal{L}_{\text{int}} = -Y_N\overline{F}_D\phi^\dagger E_S - Y_{fi}\overline{L}_i F_D S + h.c. \quad (4)$$

D_μ stands for the corresponding covariant derivative of the doublet and singlet fermions. The SM Higgs potential is given by, $V^{SM}(\phi) = -m^2\phi^2 + \lambda\phi^4$, with, $\phi = (G^+, \frac{H+v+iG}{\sqrt{2}})^T$ is the SM Higgs doublet. G 's stand for the Goldstone bosons and $v = 246.221$ GeV being the vacuum expectation value of the Higgs H fields. The charged component of the fermion doublet (E_D^\pm) and the singlet charged fermion (E_S^\pm) mix at tree level. The mass matrix for these charged fermion fields is given by,

$$\mathcal{M} = \begin{pmatrix} M_{ND} & M_X \\ M_X^\dagger & M_{NS} \end{pmatrix}. \quad (5)$$

where, $M_X = \frac{Y_N v}{\sqrt{2}}$. The mass eigenstates are obtained by diagonalizing the mass matrix with a rotation of the (E_D^\pm E_S^\pm) basis,

$$\begin{pmatrix} E_1^\pm \\ E_2^\pm \end{pmatrix} = \begin{pmatrix} \cos\beta & \sin\beta \\ -\sin\beta & \cos\beta \end{pmatrix} \begin{pmatrix} E_D^\pm \\ E_S^\pm \end{pmatrix} \quad (6)$$

The mixing angle (β) between the fermions can be written as,

$$\tan 2\beta = \frac{2M_X}{M_{NS} - M_{ND}}$$

Diagonalization of eqn. 5 gives the following eigenvalues for the charged leptons ($M_{NS} - M_{ND} \gg M_X$) as,

$$M_{E_1^\pm} = M_{ND} - \frac{2(M_X)^2}{M_{NS} - M_{ND}},$$

$$M_{E_2^\pm} = M_{NS} + \frac{2(M_X)^2}{M_{NS} - M_{ND}}.$$

The masses of the neutral fermion scalar fields can be calculated as,

$$M_{X_1^0} = M_{ND}, \quad M_S^2 = \frac{m_S^2 + kv^2}{2}, \quad M_H^2 = 2\lambda v^2.$$

Hence, in this model, neutral fermion can not serve as the DM candidate as $M_{E_1^\pm} < M_{X_1^0} < M_{E_2^\pm}$. Only the scalar fields S for $M_S < M_{E_1^\pm}$ can behave as a viable DM candidate. We keep $M_{E_2^\pm} = 1500$ GeV and $\cos\beta = 0.995$ fixed through out the analysis and will discuss the detailed discussion on the new region of the allowed parameter spaces and the effect of the presence of additional Z_2 -odd fermion in the dark matter section IV A.

The parameter space of this model is constrained by various bounds arising from theoretical considerations like absolute vacuum stability and unitarity of the scattering matrix and observation phenomenons like dark matter relic density and baryogenesis. Also, the LHC puts severe constraints on this model. In the following section, the constraints on the model will be discussed.

III. CONSTRAINTS ON THIS MODELS

A. Constraints on scalar potential couplings from stability, perturbativity and unitarity

Most severe constraints come from the ‘bounded from below’ of the potential, which ensure the absolute stability of the electroweak vacuum. The potential bounded from below signifies that there is no direction in field space along which the potential tends to minus infinity. In unitary gauge, for $H, S \gg v$, the scalar potential of equation (2) can be further simplified as,

$$V(H, S) = \frac{1}{4} \left\{ \sqrt{\lambda}H^2 + \sqrt{\frac{\lambda_S}{6}}S^2 \right\}^2 + \frac{1}{4} \left\{ \kappa + \sqrt{\frac{2\lambda\lambda_S}{3}} \right\} H^2 S^2. \quad (7)$$

The necessary conditions for the scalar potential are given by,

$$\lambda(\Lambda) > 0, \quad \lambda_S(\Lambda) > 0 \quad \text{and} \quad \kappa(\Lambda) + \sqrt{\frac{2\lambda(\Lambda)\lambda_S(\Lambda)}{3}} > 0.$$

Here, all the coupling constants in this model are evaluated at a scale Λ using RG equations [41]. However, these conditions become nonfunctional if the Higgs

quartic coupling λ becomes negative at some energy scale to contribute the electroweak vacuum metastable. In this situation, we need to handle metastability constraints on the potential differently, shown in Ref. [42]. In addition, for the radiatively improved Lagrangian of our model to be perturbative, we have [43, 44],

$$\lambda(\Lambda) < \frac{4\pi}{3}; \quad |\kappa(\Lambda)| < 8\pi; \quad |\lambda_S(\Lambda)| < 8\pi. \quad (8)$$

The couplings of the scalar potential (λ, κ and λ_S) of this model are constrained by the unitarity of the scattering matrix (S-matrix). At very high field values, one can obtain the S-matrix by using various scalar-scalar, gauge boson-gauge boson, and scalar-gauge boson scatterings. Using the equivalence theorem, we reproduced the S-matrix for this model. The unitarity demands that the eigenvalues of the S-matrix should be less than 8π . The unitary bounds are given by [44],

$$\lambda \leq 8\pi \quad \text{and} \quad \left| 12\lambda + \lambda_S \pm \sqrt{16\kappa^2 + (-12\lambda + \lambda_S)^2} \right| \leq 32\pi.$$

B. LHC diphoton signal strength bounds

At one-loop level, the physical charged fermion E_1^\pm and E_2^\pm add extra contribution to the decay width as,

$$\Gamma(H \rightarrow \gamma\gamma) = A \left| \sum_i Q_i^2 Y_{Ni} F_{1/2}(\tau_{E_i^\pm}) + C \right|, \quad (9)$$

where, $A = \frac{\alpha^2 M_h^3}{256\pi^3 v^2}$, C is the SM contribution, $C = \sum_f N_f^c Q_f^2 y_f F_{1/2}(\tau_{E_i^\pm}) + y_W F_1(\tau_W)$ and $\tau_x = \frac{M_H^2}{M_x^2}$. Q denote electric charge of corresponding particles and N_f^c is the color factor. Higgs H coupling to $f\bar{f}$ and WW is denoted by y_f and y_W . $Y_{N1} = \sqrt{2} \cos\beta \sin\beta Y_N$ and $Y_{N2} = -\sqrt{2} \cos\beta \sin\beta Y_N$ stand for corresponding couplings $H E_i + E_i^-$ ($i = 1, 2$) and the loop function $F_{(0,1/2,1)}(\tau)$ can be found in Ref [45]. In this analysis, we find that $M_{E_{1,2}^\pm} > 200$ GeV for $Y_N = \mathcal{O}(1)$ is still allowed from the LHC di-photon signal strength $\mu_{\gamma\gamma} = \frac{\Gamma(H \rightarrow \gamma\gamma)_{BSM}}{\Gamma(H \rightarrow \gamma\gamma)_{SM}}$ data. It is similarly true for $\mu_{Z\gamma}$ as $\cos\beta \sim 1$ in this model.

C. Bounds from electroweak precision experiments

Beyond the EW scale, electroweak precision bounds are affected by the presence of extra virtual particles in loops through vacuum polarization correction. Bounds from electroweak precision experiments are added in new physics contributions via self-energy parameters

S, T, U from EW precision experiments does put bounds on new physics contributions [46, 47]. The S and T parameters allows the new physics contributions to the neutral and the difference between neutral and charged weak currents respectively. However, the U parameter is only sensitive to the mass and width of the W -boson, thus in some cases, this parameter is neglected. The NNLO global electroweak fit results from the Gfitter group [46], $\Delta S_{BSM} < 0.05 \pm 0.11$, $T_{BSM} < 0.09 \pm 0.13$ and $\Delta U_{BSM} < 0.011 \pm 0.11$. In this model, a very small mass difference $\Delta M \sim 20$ GeV between the charged and neutral fermions of the doublet F_D [47, 48] with $M_N > 200$ GeV and heavy singlet charged fermion mass $\mathcal{O}(1)$ TeV are considered to evade these bounds.

D. Dark matter

The lightest stable Z_2 odd particle in our model S , behaves as proper DM candidate in our model. As per our choice of parameter space, DM relic density constraints should satisfy current results from Planck and WMAP [49],

$$\Omega_{DM} h^2 = 0.1198 \pm 0.0012 \quad (10)$$

Recent direct-detection experiments like the Xenon-1T [10] and invisible Higgs decay width data including indirect Fermi-LAT data have restricted the arbitrary Higgs portal coupling and the dark matter mass [42, 50]. It is also possible to explain various observations in the indirect DM detection experiments from this model. However, we do not discuss it here, as these estimations involve proper knowledge of the astrophysical backgrounds and an assumption of the DM halo profile which contains some arbitrariness.

In our study we use `FeynRules` [51] along with `micrOMEGAS` [52] to compute the relic density of the scalar DM. A comprehensive discussion on DM has been carried out in the numerical analysis section.

E. Lepton flavor violation and Baryogenesis

It is well-known lepton flavor violation (LFV) processes put severe constraints on the LFV couplings and in general on the model parameter space. The size of the LFV is controlled by the lepton number violating couplings Y_{fi} ($i = 1, 2, 3$). Since the observed dark matter abundance is typically obtained for $\kappa = \mathcal{O}(0-1)$ and $Y_{fi} = \mathcal{O}(0-1)$ through s -channel, t -channel annihilation and the combination of these two processes (co-annihilation, i.e., mass differences can also play a crucial role), the lepton flavor observable are expected to

give additional stringent constraints. Among the various LFV processes, the radiative muon decay $\Gamma(\mu \rightarrow e\gamma)$ is most popular and restrictive one, which in the present model is mediated by charged particles E_1^\pm, E_2^\pm present in the internal lines of the one-loop diagram 1. The cor-

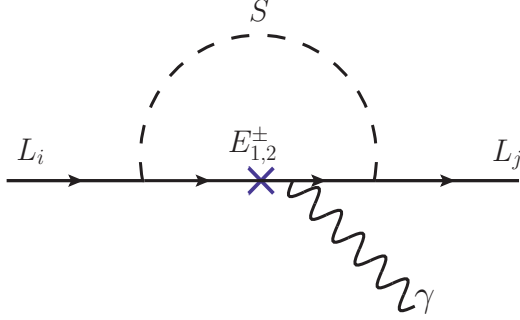


FIG. 1: LFV process by the radiative $\mu \rightarrow e\gamma$ decay.

responding expression for the branching ratio is given by,

$$\text{BR}(\mu \rightarrow e\gamma) = \frac{3\alpha_{em}}{64\pi G_F^2} \left| \cos^2 \beta Y_{f1}^\dagger Y_{f2} \frac{F(M_{E_1^\pm}^2/M_S^2)}{M_S^2} + \sin^2 \beta Y_{f1}^\dagger Y_{f2} \frac{F(M_{E_2^\pm}^2/M_S^2)}{M_S^2} \right|^2 \quad (11)$$

where, $F(x) = \frac{x^3 - 6x^2 + 3x + 2 + x \ln(x)}{6(x-1)^4}$.

The most recent experimental bounds for LFV could be found in Ref. [53]. Throughout this analysis we keep fixed $Y_{f2} = \mathcal{O}(10^{-3})$ and put constraints to the other parameters from the flavor violating decay [53] $\text{BR}(\mu \rightarrow e\gamma) < 4.2 \times 10^{-13}$ at 90% CL.

Our motivation is also to check the validity of baryogenesis produced via the mechanism of thermal leptogenesis. The lightest vectorlike fermion E_1^- is decaying to a lepton and the scalar singlet S , which eventually produces the desired lepton asymmetry in our model. The interactions of E_1^- violate lepton number (L) because L cannot be consistently assigned to F_D, E_S . We focus on the decay and inverse decay of the charged particle (E_1^-) of the fermion sector into a lepton and dark matter, corresponding to lepton number violation by $\Delta L = 2$ via the wash-out processes. The asymmetries generated by E_1^- decay dominated the whole process by the strong wash-out processes over the asymmetries generated by the other particles like X_1^0, E_2^- . In standard thermal leptogenesis scenario, the decay parameter plays a significant role to distinguish between weak and strong washout regime. Decay parameter is the ratio between decay width of the decaying VLF to the Hubble

constant at $T = M_{E_1^\pm}$, which is expressed as,

$$K = \frac{\Gamma_1}{H(T = M_{E_1^\pm})} = \frac{(A_{f1}^\dagger A_{f1}) M_{E_1^\pm}}{8\pi} \frac{M_{Planck}}{1.66\sqrt{g_*} M_{E_1^\pm}^2}, \quad (12)$$

where, $\Gamma_1 = \frac{(A_{f1}^\dagger A_{f1}) M_{E_1^\pm}}{8\pi}$ and the Hubble constant at $T = M_{E_1^\pm}$ is defined as $H(T = M_{E_1^\pm}) = \frac{M_{Planck}}{1.66\sqrt{g_*} M_{E_1^\pm}^2}$.

M_{Planck} is the the Planck mass ($\simeq 1.22 \times 10^{19}$ GeV) and g^* is the effective number of degree of freedom which is approximately $g^* \sim 110$ for two VLF case. We used the parameterization of the Yukawa matrix *w.r.t.* the mixing angle β , as $A_{fi} = Y_{fi} \cos \beta$ and $B_{fi} = Y_{fi} \sin \beta$. The regime is considered to be in weak washout if $K \lesssim 1$ while for $K \gtrsim 10^6$ is considered to be a strong washout regime. The region in between them is considered to be a strong washout regime. This washout factor K evoke the parameterization of dilution factor k , which can be found in [17].

Next, we check the CP asymmetry produced by the

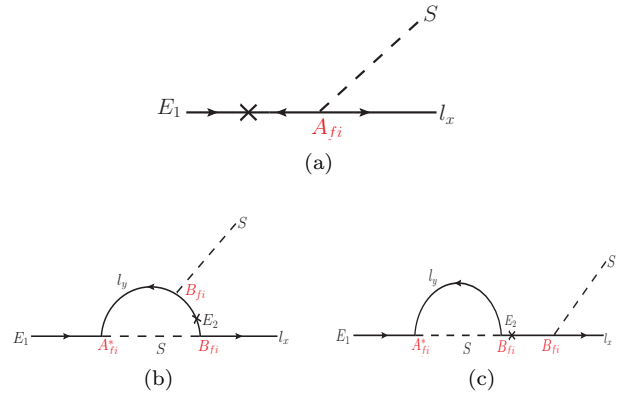


FIG. 2: Lepton asymmetry generation in tree as well as in loop level. In these lepton number violating processes, the \times in the fermionic line represents the mass insertion of the respective particle and $l_{x,y}$ represents the lepton flavor generation. A_{fi} and B_{fi} are the parameterized elements of the Yukawa coupling matrix.

LVF process in our model. To produce non-vanishing lepton asymmetry, the decay of E_1^\pm must have lepton number violating process with different decay rates to a final state with particle and anti-particle. Asymmetry in lepton flavor α produced in the decay of E_1^\pm , defined

as,

$$\epsilon_{xx} = \frac{\Gamma(E_1^- \rightarrow l_x^- S) - \Gamma(E_1^+ \rightarrow \overline{l_x^-} S)}{\Gamma(E_1^- \rightarrow l^- S) + \Gamma(E_1^+ \rightarrow \overline{l^-} S)}, \quad (13)$$

where, $\overline{l_x^-}$ is the antiparticle of l_x^- and S is the dark matter candidate in our model.

Following the calculation for non-degenerate RH mass¹, from the work of [17], we obtain the asymmetry term as,

$$\epsilon_{xx} = \frac{1}{8\pi} \frac{1}{(A_{f1}^\dagger A_{f1})} \sum_j \text{Im}\{(A_{fi}^*)(A_{fx}^\dagger B_{fx})_{1j} B_{fj}\} g(p_j) + \frac{1}{8\pi} \frac{1}{(A_{f1}^\dagger A_{f1})} \sum_j \text{Im}\{(A_{fi}^*)(A_{fx}^\dagger B_{fx})_{1j} B_{fi}\} \frac{1}{1-p_j}. \quad (14)$$

Here, $p_j \equiv \frac{M_j^2}{M_1^2}$ and within the SM $g(p_j)$ is defined as,

$$g(p_j) = \sqrt{p_j} \left(\frac{2 - p_j - (1 - p_j^2) \ln(1 + p_j/p_j)}{1 - p_j} \right). \quad (15)$$

If we take sum over the final state flavor x , neglecting the flavor effect, the second line from equation (14) violates the single lepton flavors, however, it conserves the total lepton number. Hence it will not contribute to the total CP-asymmetry. Thus the total CP-asymmetry produced by the tree-level and one-loop level is given by,

$$\epsilon_{11} \equiv \sum_x \epsilon_{xx} = \frac{1}{8\pi} \frac{1}{(A_{f1}^\dagger A_{f1})} \text{Im}[(A_{f2}^\dagger B_{f1})]^2 g(p_2). \quad (16)$$

The total baryon asymmetry generated is read as,

$$Y_B = ck \frac{\epsilon_{11}}{g_*}. \quad (17)$$

Where c and k are the conversion factor and dilution factor respectively. We consider the effective relativistic degrees of freedom to be $g = 110.75$, slightly higher than that of the SM contribution. Various corrections corresponding to the asymmetry generations are not discussed in this work and they are left for future study. This situation understudy is equivalent to the heavy Majorana mediated thermal leptogenesis processes, where the lightest Majorana particle is decaying to a lepton and Higgs doublet. The scale of the vector-like fermion, which undergoes the decay processes is around 500 GeV, hence low-scaled leptogenesis is applicable in our study.

F. Neutrino mass via one loop process

In this section, we will try to give a brief overview of the neutrino mass generation in one-loop level. The neutral Z_2 -odd scalar and fermion involved into the radiative neutrino mass generation after the EWSB, which is shown in Fig. 3. Summing over all the two-point

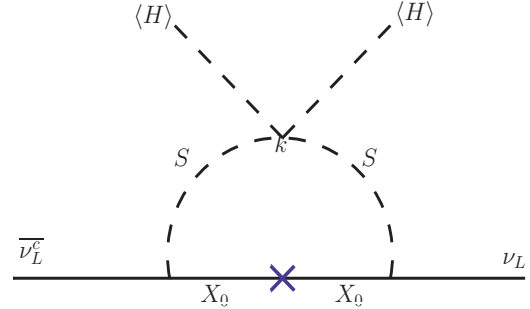


FIG. 3: One-loop contribution to neutrino mass generation with a scalar S and fermion X_1^0 .

function contributions, we arrive at the neutrino mass matrix component as [54],

$$(M_\nu)_{ij} = \frac{1}{16\pi^2} (Y_{fi}^\dagger Y_{fi}) (\kappa v^2) I(M_N, M_{DM}) \quad (18)$$

where, $i, j = 1, 2, 3$ stand for the lepton generation index. M_N is the mass for the neutral heavy fermion. $I(M_N, M_{DM})$ is the loop function, defined as [54],

$$I(M_N, M_{DM}) = 4M_N \frac{M_{DM}^2 - M_N^2 + M_N \log(\frac{M_N^2}{M_{DM}^2})}{(M_{DM}^2 - M_N^2)^2} \quad (19)$$

To get the neutrino mass eigenvalues, we have to diagonalize the above mass matrix using the well established PMNS matrix as: $m_{Diag} = U_{PMNS}^\dagger M_\nu U_{PMNS}$. It is also essential to ensure that the choice of Yukawa couplings, as well as other parameters involved in light neutrino mass, are consistent with the current neutrino oscillation data. It would be convenient to adopt the parameterize the Yukawa matrix using Casas-Ibarra parameterization [55], to be consistent with the current oscillation data.

From the above equations 18 and 19, light neutrino masses and mixing angles can be visualized by adjusting the coupling and mass parameters present in the equation (18). For a few hundred GeV dark matter and heavy neutral fermions, one can choose small κ of $\mathcal{O}(10^{-5})$ to get the small neutrino masses. One can see from Eqn. (18), in the limit $\kappa v^2 \rightarrow 0$, the light neutrino masses vanishes. This limit also signifies the fact that

¹ For degenerate mass with mass spiting equal to decay width, one have to consider resonant leptogenesis.

the vanishing neutrino masses are quite obvious as κ in the scalar potential breaks lepton number by two units, when considered together with the SM-singlet fermions Lagrangian. Hence, the smallness of κ is technically natural in the t Hooft sense [56], as adjusting $\kappa \rightarrow 0$ allows us to define global $U(1)$ lepton number symmetry. At the same time by adjusting both the real and imaginary parts of the Yukawa couplings the mixing angles could be produced. This smallness of the Higgs portal coupling enhances the allowed region of the parameter space and the relic density could produce via the other channels which we will discuss in detail in the dark matter numerical analysis section. The analysis of neutrino mass carried out in this work is more of a perfunctory rather than being comprehensive. The relation between dark matter mass and neutrino mass matrix is established in Eqn. (18). One can scan over the parameter space by adjusting the couplings and analysis neutrino phenomenology in details as per current experimental demands.

IV. NUMERICAL ANALYSIS

A. Dark matter

As pointed out in the previous section, the viable DM candidate in this model is the lightest Z_2 -odd singlet scalar S . The production mechanism of this DM candidate depends upon the Higgs portal couplings κ through s -channel and p -channels (see Figs. 8-(a), 8-(b) and 8-(c)). It is to be noted that in the presence of the Yukawa couplings Y_{fi} and Y_N , a huge improvement to the region of the dark matter parameter space is noticed here in this model. It was not been discussed in the literature previously which motivates us to study this model. Depending upon the size of the Yukawa couplings Y_{fi} , one can get a dominant DM annihilation through t - and u -channels (see Fig. 8-(d)) in our model. The interference between the s - and p -channel and t, u -channels also played a crucial role to achieve the correct DM density. The co-annihilation channels (e.g., see Fig. 5) also played an important role to get a viable region of allowed dark matter parameter space.

It is already evident that if we neglect the effect of other Z_2 -odd fermions, i.e., annihilation through t -channels and other co-annihilation processes, a very small *low*-DM mass region around $55 < M_{DM} < 70$ for Higgs portal coupling $\kappa \sim 0.005$ is giving the exact relic density, allowed by the direct detection [10] and LHC data. The main dominant channels for *low*-DM mass region is $SS \rightarrow b\bar{b}$. For $M_{DM} > 100$ GeV, $SS \rightarrow VV$, where $V = W^\pm, Z$ gauge bosons [57]

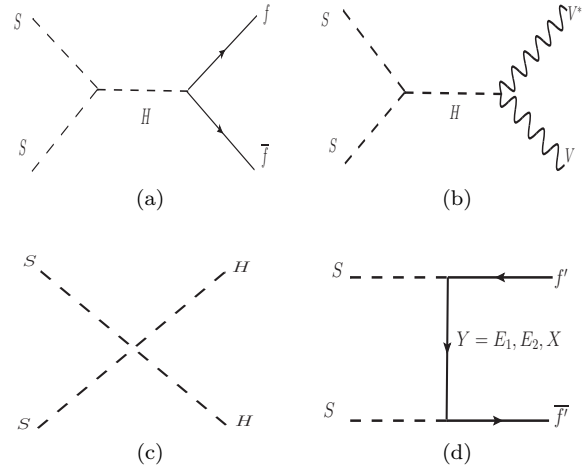


FIG. 4: The DM annihilation diagrams give the relic density. V stands for gauge bosons W, Z , f' represents the SM leptons and f are SM leptons and quarks.

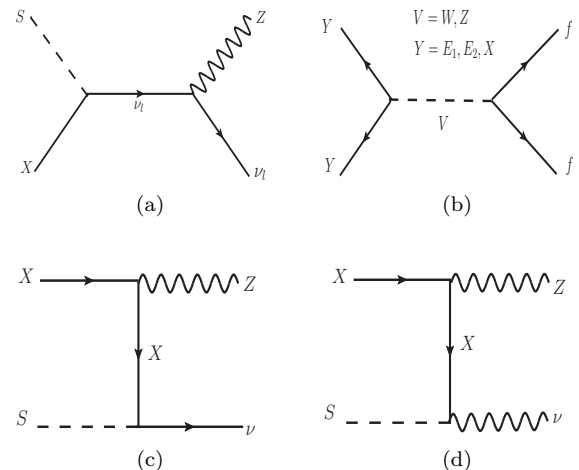


FIG. 5: The Co-annihilation and annihilation diagrams of the DM and the other Z_2 -odd fermion fields. f are SM leptons and quarks.

dominates over other DM annihilation channels. Under the approximation $M_{DM} \gg M_V, M_H$, in the non-relativistic limit one can get the DM annihilation cross-section as $\sigma(SS \rightarrow W^+W^-) \propto \frac{k^2}{M_{DM}^2}$. The allowed relic density (dominated by s - and p -channels only) for the *high*-DM mass region in $\kappa - M_{DM}$ plane is displayed in Fig. 6. We also present corresponding benchmark points BP-1a and the percentage of differ-

ent annihilation channel's contributions in the Tab. II. As usual, the main dominant channels are $SS \rightarrow YY$ with $Y = W, Z$ and H for the *high*-DM mass region. Between the color lines, we marked the allowed region

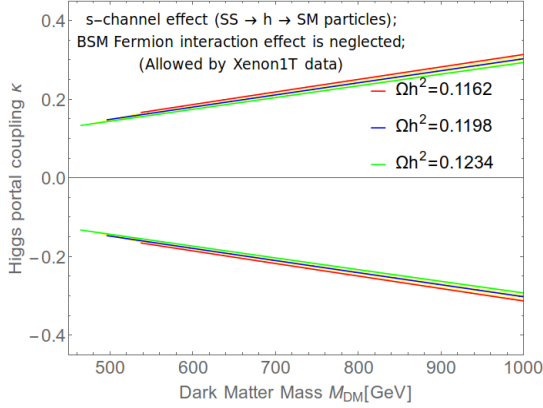


FIG. 6: The dark matter relic density through s - and p - channels only, with direct detection and other theoretical and experimental constraints. The Yukawa couplings Y_{fi} and Y_N are taken to be zero.

ensuing from relic density constraints. The green lines stand for $\Omega h^2 = 0.1234$ (upper limit at 3σ) whereas red lines corresponds $\Omega h^2 = 0.1162$ (lower limit at 3σ). One can get the exact relic density for the DM-mass region $70 < M_{DM} < 450$, however it is ruled out by the present direct detection cross-section [10]. So far we

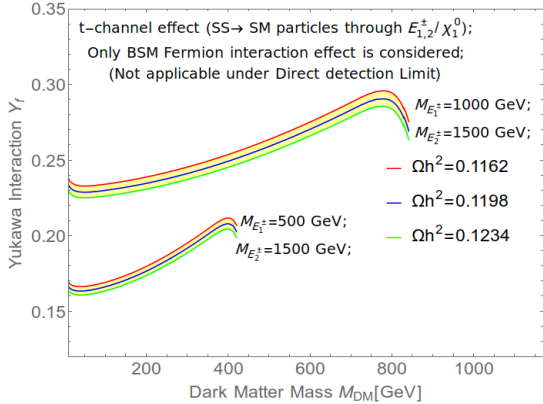


FIG. 7: The dark matter relic density through t - channels only, with direct detection and other theoretical and experimental constraints. The Higgs portal couplings κ is taken to be zero.

do not have any direct signature of the DM in the direct detection experiments, which suggest that we may

have the dark matter with a *tiny* or *zero* Higgs portal coupling and the remaining effective cross-section $< \sigma_{eff} v >$ can be adjusted by the other annihilation and co-annihilation processes to achieve the exact dark matter density. In this model, we considered such scenarios to achieve the goals.

For example, for various dark matter masses, one can get the exact density with vanishing Higgs portal coupling (κ) by adjusting the charged fermion mass and Yukawa couplings Y_{fi} . We portrait such variation in $Y_f - M_{DM}$ plane in Fig. 7 for two different values of charged fermion mass $M_{E_1^\pm} = 500$ GeV and $M_{E_1^\pm} = 1000$ GeV. We also consider $Y_{f1} = Y_{f3} = Y_f$ and $Y_{f2} = \mathcal{O}(10^{-3})$ to avoid the flavor violating decay processes (see eqn. 11). The dynamical reasons for such choice of coupling parameters lie somewhere else which is out of the scope of this paper. It can be noticed from Fig. 7 that one could get exact relic density for the dark matter mass as low as $M_{DM} = 10$ GeV. As $\kappa = 0$, the parameter space $M_{DM} < \frac{M_H}{2}$ is not restricted by the Higgs decay width and direct detection cross-section constraints. These data points also passed through other experimental constraints such as Higgs signal strength, electroweak precision test (EWPT) and theoretical bounds, viz., stability, unitarity, etc. The main dominant t, u -channel annihilation processes are $SS \rightarrow \nu\nu$ (see BP-b1,b2 and b3 in Tab. II) and $SS \rightarrow ll$, where $l = e, \tau$ and $\nu = \nu_e, \nu_\tau$ only as $Y_{f2} = \mathcal{O}(10^{-3})$.

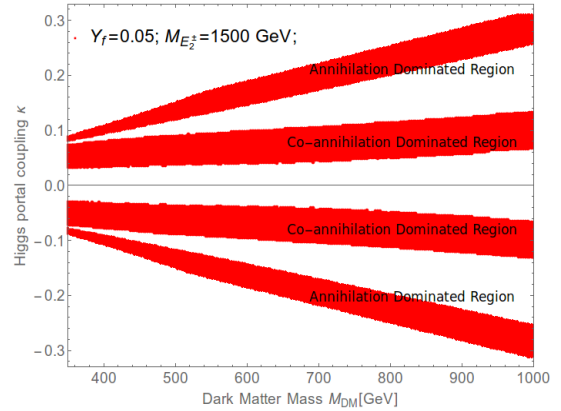


FIG. 8: The coupling $y_f = 0.05$ and second charged fermion mass $M_{E_2^\pm} = 1500$ GeV are fixed. M_{DM} , κ and $M_{E_1^\pm}$ parameters are varied in this plot. These red points satisfy the relic density at 3σ C.L. with $\Omega h^2 = 0.1198 \pm 0.0012$, satisfying all the theoretical and experimental bounds.

We now perform scans over the three dimensional parameter space. The mass parameter $M_{E_1^\pm}$ is varied from

Channel	M_{DM} (GeV)	κ	$M_{E_1^\pm}$ (GeV)	$Y_f = Y_{f1,f3}$	$\Omega_{DM}h^2$	Percentage
BP-a1	570	0.1703	2000	0.0	0.1198	$\sigma(SS \rightarrow W^\pm W^\mp)$ 47% $\sigma(SS \rightarrow HH)$ 24% $\sigma(SS \rightarrow ZZ)$ 23% $\sigma(SS \rightarrow t\bar{t})$ 6%
BP-b1	10	0.0	500	0.1665	0.1198	$\sigma(SS \rightarrow \nu\nu)$ 98% $\sigma(SS \rightarrow ll)$ 2%
BP-b2	60	0.0	500	0.1640	0.1198	$\sigma(SS \rightarrow \nu\nu)$ 98% $\sigma(SS \rightarrow ll)$ 2%
BP-b3	100	0.0	500	0.1677	0.1198	$\sigma(SS \rightarrow \nu\nu)$ 98% $\sigma(SS \rightarrow ll)$ 2%

TABLE II: The benchmark points allowed by all the theoretical and experimental constraints. The density of the dark matter S is dominated by either s - or t , u -channel annihilation processes.

200 GeV (to avoid the experimental constraints) to 1000 GeV with a step size 0.25 GeV and κ from -0.35 to 0.35 with a step size 0.002. The dark matter mass M_{DM} from ~ 200 GeV to 1000 GeV with a step size 2 GeV. For $\Delta M^{\pm,0} < 0.1M_{DM}$ [58] ($\Delta M^\pm = M_{E_1^\pm} - M_{DM}$ and $\Delta M^0 = M_N - M_{DM}$), the co-annihilation channels play an important role for the dark matter density calculation. We fixed the coupling Y_f at 0.05 to reduce the t , u -channel annihilation contributions in the relic density. The effect is almost negligible for the second charged fermion mass $M_{E_2^\pm} = 1500$ GeV and $\cos\beta = 0.995$. These parameters play an important role to get the baryon asymmetry of the Universe. In Fig. 8, we display the allowed parameters in the $\kappa - M_{DM}$ plane. These red points satisfy the relic density at 3σ C.L. with $\Omega h^2 = 0.1198 \pm 0.0012$. The two middle bands close to $|\kappa| \sim 0.03 - 0.10$ are mainly dominated by the co-annihilation channels. For example, we present two such benchmark points (BP-c1 and BP-c2) and the corresponding contributions in Tab. III. The other two bands dominated by the annihilation of the dark matter through $s + p$ - as well as $t + u$ -channels. Large Higgs portal coupling, such as $\kappa = 0.148$ (BP-c4) are mainly dominated by the $s + p$ -channel annihilation processes. However, the relic density for the point BP-c3 is coming due to the combined contributions of $s + p$ - and $t + u$ -channels.

We also scans in the other three dimensional parameter space. The dark matter mass M_{DM} is varied from 5 GeV to 540 GeV and κ from -0.35 to 0.35 with a step size 0.002 and Y_f from -0.35 to 0.35 GeV with a step size 0.005 GeV with fixed $M_{E_1^\pm} = 500$ GeV. It is noted that the co-annihilation effect are completely absent here as $\Delta M^{\pm,0} > 0.1M_{DM}$. We display the allowed parameters $\kappa - M_{DM}$ plane in Fig. 9. One can

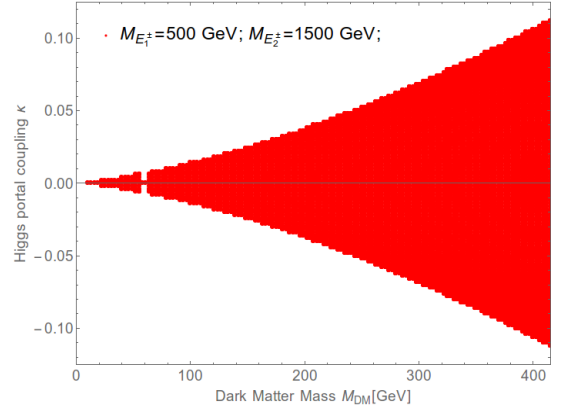


FIG. 9: The first and second charged fermion masses $M_{E_1^\pm} = 500$ GeV and $M_{E_2^\pm} = 1500$ GeV are fixed. M_{DM} , κ and y_f parameters are varied in this plot. These red points satisfy the relic density at 3σ C.L. with $\Omega h^2 = 0.1198 \pm 0.0012$ and pass all the theoretical and experimental bounds.

see, in the presence of DM annihilation via t , u -channel as most of the region is giving the correct DM density which is also allowed by other experimental constraints. For $\kappa \neq 0$, the s -channel annihilation dominates near Higgs resonance region $\sim \frac{M_H}{2}$. This region gives overabundance of dark matter density in our study. For a small $\kappa \sim 0$, the $t + u$ -channels helps to get the correct relic density at 3σ C.L. We show the $\kappa - Y_f$ plane in Fig. 10 for the same data points as in Fig. 9. We get two circular ring-type structures here. The empty region violates one of the constraints such as relic density of the dark matter, direct detection and Higgs decay width for the DM mass $< \frac{M_H}{2}$. However, in the pres-

Channel	M_{DM} (GeV)	κ	$M_{E_1^\pm}$ (GeV)	$Y_f = Y_{f1,f3}$	$\Omega_{DM} h^2$	Percentage
BP-c1	501	-0.0384	582	-0.05	0.1233	$\sigma(SS \rightarrow W^\pm W^\mp)$ 4% $\sigma(SS \rightarrow HH)$ 2% $\sigma(SS \rightarrow ZZ)$ 2% $\sigma(E_1^\pm E_1^\pm \rightarrow W^\pm W^\pm)$ 65% $\sigma(E_1^\pm E_1^\mp \rightarrow ZH)$ 20% $\sigma(E_1^\pm E_1^\pm \rightarrow t\bar{t})$ 3%
BP-c2	501	-0.087	586.2	-0.05	0.1162	$\sigma(SS \rightarrow W^\pm W^\mp)$ 19% $\sigma(SS \rightarrow HH)$ 10% $\sigma(SS \rightarrow ZZ)$ 9% $\sigma(SS \rightarrow t\bar{t})$ 3% $\sigma(E_1^\pm E_1^\pm \rightarrow W^\pm W^\pm)$ 42% $\sigma(E_1^\pm E_1^\mp \rightarrow ZH)$ 13% $\sigma(E_1^\pm E_1^\pm \rightarrow t\bar{t})$ 2%
BP-c3	501	-0.122	589.5	-0.05	0.1234	$\sigma(SS \rightarrow W^\pm W^\mp)$ 26% $\sigma(SS \rightarrow HH)$ 15% $\sigma(SS \rightarrow ZZ)$ 13% $\sigma(SS \rightarrow t\bar{t})$ 4% $\sigma(E_1^\pm E_1^\pm \rightarrow W^\pm W^\pm)$ 30% $\sigma(E_1^\pm E_1^\mp \rightarrow ZH)$ 9% $\sigma(E_1^\pm E_1^\pm \rightarrow t\bar{t})$ 1%
BP-c4	501	-0.148	595	-0.05	0.1166	$\sigma(SS \rightarrow W^\pm W^\mp)$ 44% $\sigma(SS \rightarrow HH)$ 26% $\sigma(SS \rightarrow ZZ)$ 22% $\sigma(SS \rightarrow t\bar{t})$ 7%

TABLE III: The benchmark points allowed by all the theoretical and experimental constraints. The density of the dark matter S is dominated by either annihilation or co-annihilation or combined effect of these processes.

ence of the co-annihilation processes with/or a different choice of the $M_{E_1^\pm}$ the gaps between these two circular rings could be filled. We also display a similar plots in $\kappa - M_{DM}$ and $\kappa - Y_f$ planes in Figs. 11 and 12 for the $M_{E_1^\pm} = 1000$ GeV, where we change the variation for DM mass M_{DM} from 5 GeV to 1000 GeV. We get a similar type of plot with a large region of the parameter spaces allowed by all the experimental and theoretical constraints. Few BMPs and their corresponding contributions are presented in Tab. IV. $\sigma(SS \rightarrow \nu\nu)$ is mainly dominated by the $t + u$ -channel annihilation processes whereas $\sigma(SS \rightarrow YY)$, $Y = W, Z, H, t$ dominated by the $s + p$ -channel annihilation processes.

B. Baryon asymmetry and Neutrino

In this minimal model, with the choice of parameter space, we try to give some numerical insights to neutrino phenomenology and baryogenesis. Using equation

(18), with the masses for subsequent fields $M_{DM} = 700$ GeV $M_N = 1000$ GeV and choice of Yukawa parameters $|Y_{f1}| = 0.4, |Y_{f2}| = 10^{-4}, |Y_{f3}| = 0.157$, we get the sum of the neutrino masses of the order of sub-eV range (~ 0.12 eV) for Higgs portal coupling $\kappa < 10^{-5}$. This tiny κ is directly associated with dark matter relic density via the t -channel process. We are able to generate mixing angles $\theta_{12} = 32.7^\circ$, $\theta_{13} = 8.4^\circ$, $\theta_{23} = 44.71^\circ$ and mass differences $\Delta m_{21}^2 = 7.31 \times 10^{-5}$ and $\Delta m_{31}^2 = 2.63 \times 10^{-4}$ with phases $\alpha = \delta = 45^\circ$. Although Δm_{21}^2 is within the present 3σ bound however, Δm_{31}^2 is slightly deviate from the actual range. This inconsistency can be resolved by introducing one extra field into the model. We can play with other parameters to get the correct experimental values for the light neutrinos.

We also checked the ability of this model to explain the baryogenesis via thermal leptogenesis. We worked out the low-scale leptogenesis within a strong wash-out regime. One can understand that the source of CP-violation from Fig. 2 and corresponding Eqns. 13-

Channel	M_{DM} (GeV)	κ	$M_{E_1^\pm}$ (GeV)	$Y_f = Y_{f1,f3}$	$\Omega_{DM} h^2$	Percentage
BP-d1	325	0.05	1000	0.225	0.1173	$\sigma(SS \rightarrow \nu\nu)$ 72% $\sigma(SS \rightarrow W^\pm W^\mp)$ 12% $\sigma(SS \rightarrow HH)$ 7% $\sigma(SS \rightarrow ZZ)$ 6% $\sigma(SS \rightarrow t\bar{t})$ 4%
BP-d2	500	0.05	1000	0.250	0.1219	$\sigma(SS \rightarrow \nu\nu)$ 88% $\sigma(SS \rightarrow W^\pm W^\mp)$ 5% $\sigma(SS \rightarrow ZZ)$ 3% $\sigma(SS \rightarrow HH)$ 3%
BP-d3	675	0.05	1000	0.280	0.1169	$\sigma(SS \rightarrow \nu\nu)$ 96% $\sigma(SS \rightarrow W^\pm W^\mp)$ 3% $\sigma(SS \rightarrow ZZ)$ 1% $\sigma(SS \rightarrow HH)$ 1%

TABLE IV: The benchmark points allowed by all the theoretical and experimental constraints. $\sigma(SS \rightarrow \nu\nu)$ is mainly dominated by the $t + u$ -channel annihilation processes whereas $\sigma(SS \rightarrow YY)$, $Y = W, Z, H, t$ dominated by the $s + p$ -channel annihilation processes.

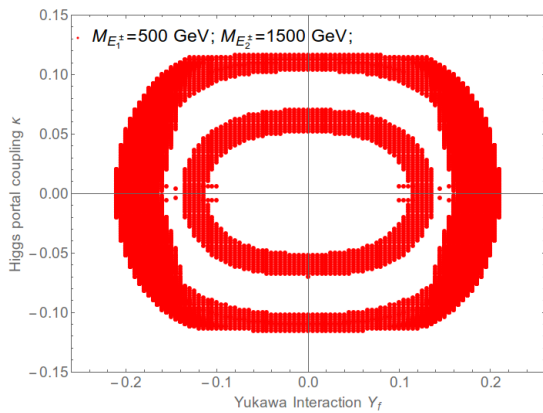


FIG. 10: The first and second charged fermion masses $M_{E_1^\pm} = 500$ GeV and $M_{E_2^\pm} = 1500$ GeV are fixed. M_{DM} , κ and y_f parameters are varied in this plot. These red points satisfy the relic density at 3σ of $\Omega h^2 = 0.1198 \pm 0.0012$ and pass all the theoretical and experimental bounds.

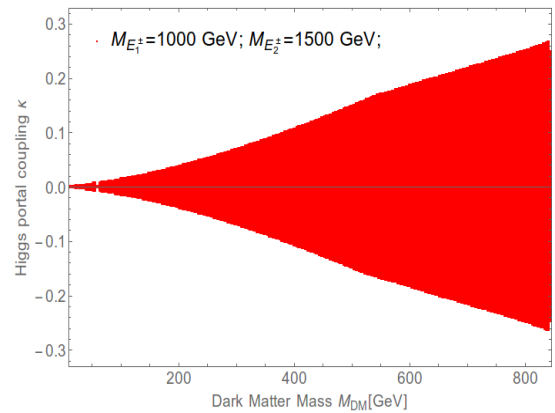


FIG. 11: The first and second charged fermion masses $M_{E_1^\pm} = 1000$ GeV and $M_{E_2^\pm} = 1500$ GeV are fixed. M_{DM} , κ and y_f parameters are varied in this plot. These red points satisfy the relic density at 3σ of $\Omega h^2 = 0.1198 \pm 0.0012$ and pass all the theoretical and experimental bounds.

16. We adopted the numerical formalism from [17, 28] to carry-out our numerical analysis. The allowed region with correct baryon asymmetry value is shown in Fig. 13 in the $\text{Im}[Y_{f2}] - M_{E_1^\pm}$ plane. The purple band satisfies baryon asymmetry value at 3σ C.L. with $Y_{\Delta B} = (8.75 \pm 0.23) \times 10^{-11}$. $\text{Im}[Y_{f2}]$ is the imaginary part of the second Yukawa coupling 4. The real part of this coupling is also taken to be very small to avoid

the LFV bounds [53] (see Eqn. 11). The other parameters are fixed as $M_{E_2^\pm} = 1500$ GeV, $\cos \beta = 0.995$, $Y_f = 0.4 + 8 \times 10^{-5} i$. The dynamical reasons for the smallness of these imaginary parts of these coupling may lie somewhere else. Influence of the small Yukawa coupling Y_{f2} , that satisfies the observed baryon asymmetry value can also be found in generating neutrino mass and mixing angles. With the choice of new parameter scale

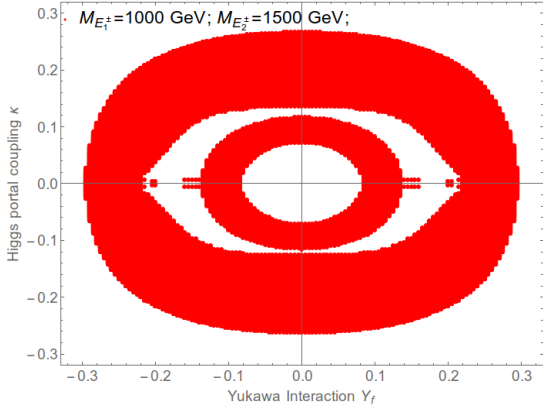


FIG. 12: The first and second charged fermion masses $M_{E_1^\pm} = 1000$ GeV and $M_{E_2^\pm} = 1500$ GeV are fixed. M_{DM} , κ and y_f parameters are varied in this plot. These red points satisfy the relic density at 3σ of $\Omega h^2 = 0.1198 \pm 0.0012$ and pass all the theoretical and experimental bounds.

and new fields, the study on various wash-out processes and complete analysis of neutrino phenomenology are left for future work.

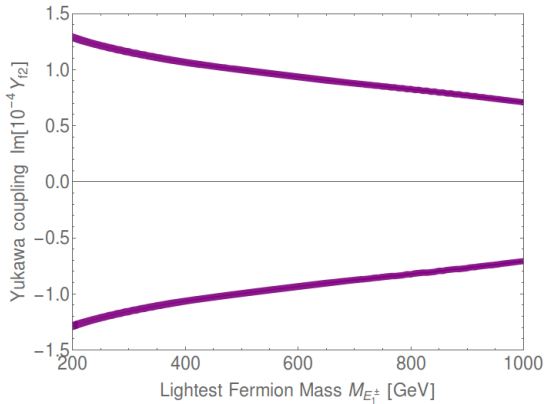


FIG. 13: The purple bands are giving the correct numbers which can explain the baryon asymmetry of the Universe.

C. Collider Searches

We perform a search for the lightest charged fermion E_1^\pm in the context of 14 TeV LHC experiments with integrated luminosity of 3000 fb^{-1} for event's process $pp \rightarrow E_1^\pm E_1^\mp$, where a SM leptons l is produced through

decays of the charged fermion as $E_1^\pm \rightarrow l^\pm S$. Hence in the final state events have two same flavors opposite sign (SFOS) leptons including significant missing transverse energy coming from the LSP S . The events are selected with two same flavors opposite sign (SFOS) isolated electron² with transverse momentum p_T larger than 30 GeV. The charged lepton isolation requires that there is no other charged particle with $p_T > 0.5$ GeV/c within a cone of $\Delta R = \sqrt{\Delta\Phi^2 + \Delta\eta^2} < 0.5$ centered on the cell-associated to the charged lepton. Besides, the ratio of the scalar sum of the transverse momenta of all tracks to p_T of the lepton (chosen for isolation) is less than 0.12 (0.25) for the electron (muon). Here p_T , Φ and η are the transverse momentum, polar angle and pseudo-rapidity of charged leptons respectively. The charged lepton candidates are required to be within a pseudorapidity range of $|\eta| < 2.5$. Number of light and b -jets in the final state are taken to be zero. The invariant mass M_{ll} and transverse missing energy distributions \cancel{E}_T can be a useful probe to search for the charged fermion E_1^\pm of this model. We show these distributions in Figs. 14 and 15 respectively for the benchmark points $\cos\beta = 0.995$, $Y_f = 0.165$, $M_{E_1^\pm} = 500$ GeV and $M_{E_2^\pm} = 1500$ GeV. Here, processes like

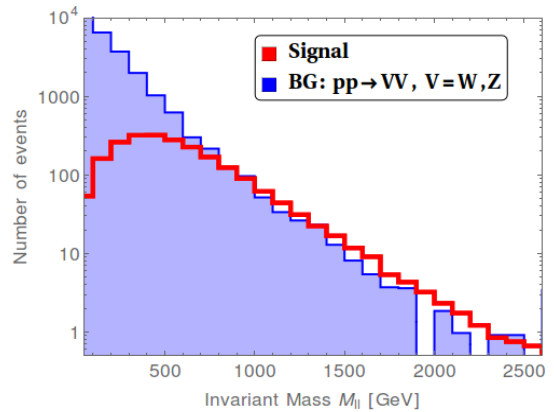


FIG. 14: The invariant mass distribution of the two same flavor opposite sign (SFOS) leptons for the signal $pp \rightarrow E_1^\pm E_1^\pm$, $E_1^\pm \rightarrow l^\pm S \rightarrow ll + \cancel{E}_T$ and $pp \rightarrow VV$, $V = W, Z$ backgrounds.

$pp \rightarrow WW$ ($W \rightarrow l\nu$), $pp \rightarrow ZW$ ($Z \rightarrow ll, W \rightarrow l\nu$) and $pp \rightarrow ZZ$ ($Z \rightarrow ll, Z \rightarrow \nu\bar{\nu}$) can add to the SM background if additional charged leptons get misidentified or remain unreconstructed. Also other reducible

² Total number of muon remains zero in the final stat events as $Y_{f2} \sim 0$

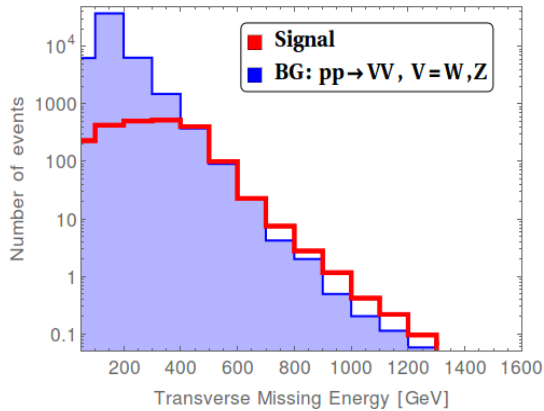


FIG. 15: The transverse mass energy distribution for the signal $pp \rightarrow E_1^\pm E_1^\pm, E_1^\pm \rightarrow l^\pm S \rightarrow ll + \cancel{E}_T$ and $pp \rightarrow VV, V = W, Z$ backgrounds.

backgrounds like $pp \rightarrow t\bar{t}, t \rightarrow Wb, W \rightarrow l\nu$ may also produce two leptons and jets in the final state. The additional cuts on number of jets reduce this background to be less than one.

For our analysis we choose the same selection cuts for the signal and background VV ($V = W, Z$) as discussed before. Further we impose $M_{ll} > 400$ GeV and $\cancel{E}_T > 400$ GeV optimization cuts to maximize the signal significance. It is found that the number of events at 14 TeV run of the LHC with luminosity $L = 3000 \text{ fb}^{-1}$ becomes around $S = 261.74$, whereas the total background attains a values of $B = 12$. We find the corresponding significance $\frac{S}{\sqrt{B}} = 75$.

V. CONCLUSION

We study the possibility of scalar singlet dark matter in the minimal scotogenic model simultaneously explaining the baryon asymmetry of the Universe through the flavor violating leptogenesis process. The structure of the model projected here uses a minimum number of field content to explain dark matter, baryogenesis as well as the neutrino observable. Apart from the SM field content, this model contains vectorlike one neutral and two charged fermions along with a singlet scalar field. In the presence of other particle (s), one can get the right relic density via co-annihilation or one may have the interaction term such that the dark matter can annihilate into SM particles through additional p, t and u -channels. The constructive or destructive interference among these channels helps to modify the effective annihilation cross-section and give the right relic density of the dark matter. These type of scenarios are observed in

our model. The vector-like fermions have an interaction term with the Higgs scalar fields for which a mass difference is generated between the degenerate neutral and charged fermions of the doublet at tree-level. The interaction term with singlet scalar helps to generate the neutrino mass and mixing angles via a 1-loop level through the radiative seesaw mechanism. Both of these interactions terms also help to get the exact relic density of the Universe for large ranges $0.1 - 300 \text{ TeV}$ ($M_{DM} \gtrsim 300 \text{ TeV}$ violates the unitary bounds [59]) of the dark matter mass. The Higgs portal coupling $\mathcal{O}(10^{-5})$ along with these Yukawa couplings $\mathcal{O}(10^{-1})$ can explain the neutrino mass and mixing angles where the relic density is achieved via the t - and u -channel annihilation or other co-annihilation processes. These new Yukawa couplings also play the lead role in explaining baryogenesis. In order to explain baryogenesis, we adopt the low-scale thermal leptogenesis mechanism, where the lightest component of the fermion doublet is decaying into a lepton and a scalar field, producing enough CP-asymmetry to produce the observed baryon asymmetry.

We also performed collider analysis to search the lightest charged fermion E_1^\pm in the context of 14 TeV LHC experiments with integrated luminosity of 3000 fb^{-1} for process $pp \rightarrow E_1^\pm E_1^\pm$ where a SM leptons l is produced through decays of the charged fermion as $E_1^\pm \rightarrow l^\pm S$. We have only analyzed the familiar $2l + \cancel{E}_T$ final states to get the signature at the future collider. The lepton final states produce relatively clean signals which are easy to identify in a hadron-rich environment like the LHC experiment. We choose benchmark points that ensure the relic density, baryon asymmetry, and neutrino parameters. We further optimized the selection cuts in order to enhance the $2l + \cancel{E}_T$ signal significance over the SM backgrounds. Our collider study showed that the dilepton final state gives promising results for the discovery of the heavy charged particle at 14 TeV LHC experiments with an integrated luminosity of 3000 fb^{-1} which may be an indication of the dark matter at the collider.

One can also put bound on the Yukawa coupling as larger Yukawa coupling may violate the stability of the scalar potential any of the direction the scalar fields at any scale (at least up to the Planck scalar $1.22 \times 10^{19} \text{ GeV}$). In this model, we work with such a choice of the Yukawa couplings and κ (especially λ_S) so that there is no new minima arise along any of the scalar field directions. In the future, we will elaborate on the details stability and/or metastability analysis for a various regions of the parameter space which could also explain all the neutrino masses and mixing angles, exact relic density and baryon-asymmetry of the Universe altogether.

In the concluding remark: if nature selects a single component WIMP dark matter candidate, which inter-

acts with the nucleus feebly through s -channel, helps to get the neutrino mass of order $\mathcal{O}(0.1)$ eV. On the assumption that the relic density can achieve via t -channel annihilation processes. We have to think of a new way to detect dark matter in the direct-detection experiments. In that case, collider searches with high luminosity are better options to detect dark matter.

VI. ACKNOWLEDGEMENT

The research work of P.D. and M.K.D. is supported by the Department of Science and Technology, Government

of India under the project grant EMR/2017/001436. NK would like to thank Dilip Kumar Ghosh for his support at IACS.

-
- [1] A. M. Sirunyan *et al.* (CMS), Phys. Lett. **B779**, 283 (2018), arXiv:1708.00373 [hep-ex].
- [2] A. M. Sirunyan *et al.* (CMS), Eur. Phys. J. **C79**, 421 (2019), arXiv:1809.10733 [hep-ex].
- [3] M. Tanabashi *et al.* (Particle Data Group), Phys. Rev. **D98**, 030001 (2018).
- [4] C. P. Burgess, M. Pospelov, and T. ter Veldhuis, Nucl. Phys. **B619**, 709 (2001), arXiv:hep-ph/0011335 [hep-ph].
- [5] N. G. Deshpande and E. Ma, Phys. Rev. **D18**, 2574 (1978).
- [6] E. Ma and D. Suematsu, Mod. Phys. Lett. **A24**, 583 (2009), arXiv:0809.0942 [hep-ph].
- [7] T. Araki, C. Q. Geng, and K. I. Nagao, Phys. Rev. **D83**, 075014 (2011), arXiv:1102.4906 [hep-ph].
- [8] E. Ma, Phys. Rev. **D73**, 077301 (2006), arXiv:hep-ph/0601225 [hep-ph].
- [9] T. Cohen, J. Kearney, A. Pierce, and D. Tucker-Smith, Phys. Rev. **D85**, 075003 (2012), arXiv:1109.2604 [hep-ph].
- [10] E. Aprile *et al.* (XENON), Phys. Rev. Lett. **121**, 111302 (2018), arXiv:1805.12562 [astro-ph.CO].
- [11] J. D. Vergados and H. Ejiri, Nucl. Phys. **B804**, 144 (2008), arXiv:0805.2583 [hep-ph].
- [12] C. Bhm, D. G. Cerdeo, P. A. N. Machado, A. Olivares-Del Campo, E. Perdomo, and E. Reid, JCAP **1901**, 043 (2019), arXiv:1809.06385 [hep-ph].
- [13] D. A. Camargo, M. D. Campos, T. B. de Melo, and F. S. Queiroz, Phys. Lett. **B795**, 319 (2019), arXiv:1901.05476 [hep-ph].
- [14] D. Restrepo, A. Rivera, M. Snchez-Pelez, O. Zapata, and W. Tangarife, Phys. Rev. **D92**, 013005 (2015), arXiv:1504.07892 [hep-ph].
- [15] A. Ahriche, A. Jueid, and S. Nasri, Phys. Rev. **D97**, 095012 (2018), arXiv:1710.03824 [hep-ph].
- [16] J. Fiaschi, M. Klasen, and S. May, JHEP **05**, 015 (2019), arXiv:1812.11133 [hep-ph].
- [17] S. Davidson, E. Nardi, and Y. Nir, Phys. Rept. **466**, 105 (2008), arXiv:0802.2962 [hep-ph].
- [18] E. Komatsu *et al.* (WMAP), Astrophys. J. Suppl. **180**, 330 (2009), arXiv:0803.0547 [astro-ph].
- [19] A. D. Sakharov, Pisma Zh. Eksp. Teor. Fiz. **5**, 32 (1967), [Usp. Fiz. Nauk161,no.5,61(1991)].
- [20] A. Strumia, in *Particle physics beyond the standard model. Proceedings, Summer School on Theoretical Physics, 84th Session, Les Houches, France, August 1-26, 2005* (2006) pp. 655–680, arXiv:hep-ph/0608347 [hep-ph].
- [21] S. Kashiwase, H. Okada, Y. Orikasa, and T. Toma, Int. J. Mod. Phys. **A31**, 1650121 (2016), arXiv:1505.04665 [hep-ph].
- [22] R. Barbieri, P. Creminelli, A. Strumia, and N. Tetradis, Nucl. Phys. **B575**, 61 (2000), arXiv:hep-ph/9911315 [hep-ph].
- [23] M. Hirsch and S. F. King, Phys. Rev. **D64**, 113005 (2001), arXiv:hep-ph/0107014 [hep-ph].
- [24] W. Buchmuller, P. Di Bari, and M. Plumacher, Annals Phys. **315**, 305 (2005), arXiv:hep-ph/0401240 [hep-ph].
- [25] P. S. B. Dev, P. Di Bari, B. Garbrecht, S. Lavignac, P. Millington, and D. Teresi, Int. J. Mod. Phys. **A33**, 1842001 (2018), arXiv:1711.02861 [hep-ph].
- [26] F. R. Klinkhamer and N. S. Manton, Phys. Rev. **D30**, 2212 (1984).
- [27] S. Blanchet and P. Di Bari, Nucl. Phys. **B807**, 155 (2009), arXiv:0807.0743 [hep-ph].
- [28] T. Hugle, M. Platscher, and K. Schmitz, Phys. Rev. **D98**, 023020 (2018), arXiv:1804.09660 [hep-ph].
- [29] E. J. Chun *et al.*, Int. J. Mod. Phys. **A33**, 1842005 (2018), arXiv:1711.02865 [hep-ph].
- [30] F. F. Deppisch, J. Harz, and M. Hirsch, Phys. Rev. Lett. **112**, 221601 (2014), arXiv:1312.4447 [hep-ph].
- [31] J. Harz, W.-C. Huang, and H. Ps, *Proceedings, International Conference on Massive Neutrinos: Flavor Mixing of Leptons and Neutrino Oscillations: Singapore, Singapore, February 9-13, 2015*, Int. J. Mod. Phys. **A30**, 1530045 (2015), [Adv. Ser. Direct. High Energy Phys.25,207(2015)], arXiv:1505.07632 [hep-ph].
- [32] F. Vissani, Phys. Rev. **D57**, 7027 (1998), arXiv:hep-ph/9709409 [hep-ph].

- [33] J. Racker, JCAP **1403**, 025 (2014), arXiv:1308.1840 [hep-ph].
- [34] D. Mahanta and D. Borah, JCAP **1911**, 021 (2019), arXiv:1906.03577 [hep-ph].
- [35] S. Fraser, E. Ma, and O. Popov, Phys. Lett. **B737**, 280 (2014), arXiv:1408.4785 [hep-ph].
- [36] A. Merle and M. Platscher, JHEP **11**, 148 (2015), arXiv:1507.06314 [hep-ph].
- [37] R. Gonzalez Felipe, F. R. Joaquim, and B. M. Nobre, Phys. Rev. **D70**, 085009 (2004), arXiv:hep-ph/0311029 [hep-ph].
- [38] C. Klein, M. Lindner, and S. Ohmer, JHEP **03**, 018 (2019), arXiv:1901.03225 [hep-ph].
- [39] P. Pal, *An Introductory Course of Particle Physics*, Taylor & Francis, 2014, .
- [40] F. Pisano and A. T. Tran, *Anomaly cancellation in a class of chiral flavor gauge models*, in *14th Brazilian Meeting on Particles and Fields Caxambu, Brazil, September 29-October 3, 1993, 1993*, .
- [41] I. Garg, S. Goswami, K. N. Vishnudath, and N. Khan, Phys. Rev. **D96**, 055020 (2017), arXiv:1706.08851 [hep-ph].
- [42] S. Khan, S. Goswami, and S. Roy, Phys. Rev. **D89**, 073021 (2014), arXiv:1212.3694 [hep-ph].
- [43] B. W. Lee, C. Quigg, and H. B. Thacker, Phys. Rev. **D16**, 1519 (1977).
- [44] G. Cynolter, E. Lendvai, and G. Pocsik, Acta Phys. Polon. **B36**, 827 (2005), arXiv:hep-ph/0410102 [hep-ph].
- [45] A. Djouadi, Phys. Rept. **459**, 1 (2008), arXiv:hep-ph/0503173 [hep-ph].
- [46] M. Baak, J. Cth, J. Haller, A. Hoecker, R. Kogler, K. Mnig, M. Schott, and J. Stelzer (Gfitter Group), Eur. Phys. J. **C74**, 3046 (2014), arXiv:1407.3792 [hep-ph].
- [47] M. E. Peskin and T. Takeuchi, Phys. Rev. **D46**, 381 (1992).
- [48] G. Cynolter and E. Lendvai, Eur. Phys. J. **C58**, 463 (2008), arXiv:0804.4080 [hep-ph].
- [49] N. Aghanim *et al.* (Planck), (2018), arXiv:1807.06209 [astro-ph.CO].
- [50] P. Athron *et al.* (GAMBIT), Eur. Phys. J. **C77**, 568 (2017), arXiv:1705.07931 [hep-ph].
- [51] A. Alloul, N. D. Christensen, C. Degrande, C. Duhr, and B. Fuks, Comput. Phys. Commun. **185**, 2250 (2014), arXiv:1310.1921 [hep-ph].
- [52] G. Blanger, F. Boudjema, A. Goudelis, A. Pukhov, and B. Zaldivar, Comput. Phys. Commun. **231**, 173 (2018), arXiv:1801.03509 [hep-ph].
- [53] A. M. Baldini *et al.* (MEG II), Eur. Phys. J. **C78**, 380 (2018), arXiv:1801.04688 [physics.ins-det].
- [54] P. Fileviez Perez and M. B. Wise, Phys. Rev. **D80**, 053006 (2009), arXiv:0906.2950 [hep-ph].
- [55] J. A. Casas and A. Ibarra, Nucl. Phys. **B618**, 171 (2001), arXiv:hep-ph/0103065 [hep-ph].
- [56] G. 't Hooft, C. Itzykson, A. Jaffe, H. Lehmann, P. K. Mitter, I. M. Singer, and R. Stora, NATO Sci. Ser. B **59**, pp.1 (1980).
- [57] J. McDonald, Phys. Rev. **D50**, 3637 (1994), arXiv:hep-ph/0702143 [HEP-PH].
- [58] K. Griest and D. Seckel, Phys. Rev. **D43**, 3191 (1991).
- [59] K. Griest and M. Kamionkowski, Phys. Rev. Lett. **64**, 615 (1990).